ADVANCED OPTICAL MATERIALS
www.advopticalmat.de

Order and Disorder in Mixed (Si, P)–N Networks $Sr_2SiP_2N_6:Eu^{2+}$ and $Sr_5Si_2P_6N_{16}:Eu^{2+}$

*Marwin Dialer, Monika M. Pointner, Sophia L. Wandelt, Philipp Strobel, Peter J. Schmidt, Lkhamsuren Bayarjargal, Björn Winkler, and Wolfgang Schnick**

In the field of nitride phosphors, which are crucial for phosphor-converted light-emitting diodes, mixed tetrahedral networks hold a significant position. With respect to the wide range of compositions, the largely unexplored (Si, P)–N networks are investigated as potential host structures. In this work, two highly condensed structures, namely $Sr_2SiP_2N_6$ and $Sr_5Si_2P_6N_{16}$ are reported to address the challenges that arise from the similarities of the network-forming cations Si^{4+} and P^{5+} in terms of charge, ionic radius, and atomic scattering factor, a multistep workflow is employed to elucidate their structure. Using single-crystal X-ray diffraction, energy-dispersive X-ray spectroscopy (EDX), atomic-resolution scanning transmission electron microscopy (STEM)-EDX maps, and straightforward crystallographic calculations, it is found that $Sr_2SiP_2N_6$ is the first ordered, and $Sr_5Si_2P_6N_{16}$ the first disordered, anionic tetrahedral (Si, P)–N network. After doping with Eu^{2+}, $Sr_2SiP_2N_6:Eu^{2+}$ shows narrow cyan emission (λ_{max} = 506 nm, *fwhm* = 60 nm/2311 cm^{-1}), while for $Sr_5Si_2P_6N_{16}:Eu^{2+}$ a broad emission with three maxima at 534, 662, and 745 nm upon irradiation with ultraviolet light is observed. An assignment of Sr sites as probable positions for Eu^{2+} and their relation to the emission bands of $Sr_5Si_2P_6N_{16}:Eu^{2+}$ is discussed.

1. Introduction

Highly condensed (oxo-)nitride networks are known for their exceptional luminescence properties when doped with Eu^{2+} and convince with high quantum efficiency, low thermal quenching, as well as chemical and thermal stability.[1,2] These properties make them an essential element in commercially available phosphors used in phosphor-converted light-emitting diodes (pcLEDs). Prominent examples of such materials are β-sialon:Eu^{2+}, (Ca, Sr)$[AlSiN_3]:Eu^{2+}$, $Sr[LiAl_3N_4]:Eu^{2+}$, and $Sr[Li_2Al_2N_2O_2]:Eu^{2+}$, which all share a common feature, the presence of a mixed tetrahedral network.[3–6] In the development of novel host structures, multiple network-forming cations (NFC) offer significant advantages. First, by introduction of highly reactive compounds like Li_3N or Mg_3N_2, refractory inert binary nitrides can be activated, as has been shown for aluminum nitride or silicon nitride.[7–9] Second, it is possible to increase the condensation degree κ (Equation 1) and thus decrease the ratio between counter cations and NFCs, defined as the cation ratio *CR* (Equation 2). This is evident in the example of nitridosilicates, where κ_{max} is limited to a value of ¾ corresponding to pure Si_3N_4 (κ = 0.75). By adding Li_3N (κ = 3) or Mg_3N_2 (κ = 1.5) we can achieve higher values for the degree of condensation, as demonstrated for $Sr[Li_2Si_2N_4]:Eu^{2+}$ and $Sr[Mg_3SiN_4]:Eu^{2+}$ (κ = 1).[10,11] This is advantageous for achieving narrow emission bands which correlates with the condensation degree and thus the rigidity of a network. However, the main advantage of mixed networks is their wide range of compositions.

This diversity is crucial, as significant changes in luminescence properties often require a complete redesign of the host structure. This led us to investigate mixed (Si, P)–N networks, as the compound classes *AE*–Si–N and *AE*–P–N (*AE* = Ca, Sr, Ba) have the most representatives among ternary nitrides. This variety suggests that their combination yields numerous compounds with new structures and luminescent properties worth investigating. This can be illustrated by plotting the cation ratio *CR*, as defined by Pritzl et al., against the condensation degree κ for known compounds (**Figure 1**).[12]

M. Dialer, M. M. Pointner, S. L. Wandelt, W. Schnick
Department of Chemistry
University of Munich (LMU)
Butenandtstraße 5–13, 81377 Munich, Germany
E-mail: wolfgang.schnick@uni-muenchen.de
P. Strobel, P. J. Schmidt
Lumileds Phosphor Center Aachen (LPCA)
Lumileds
Philipsstraße 8, 52068 Aachen, Germany
L. Bayarjargal, B. Winkler
Institute of Geosciences
Goethe-University Frankfurt
Altenhoeferallee 1, 60438 Frankfurt am Main, Germany

The ORCID identification number(s) for the author(s) of this article can be found under https://doi.org/10.1002/adom.202302668

DOI: 10.1002/adom.202302668

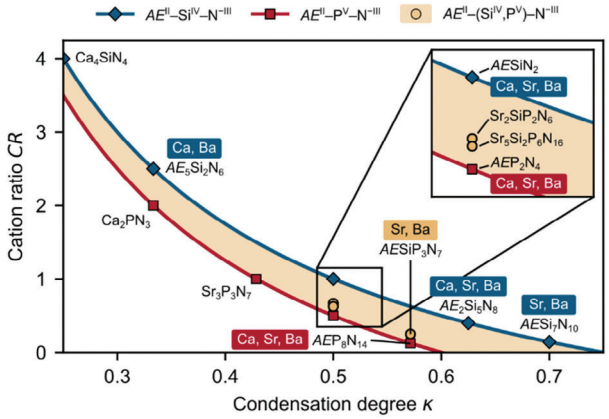

Figure 1. Graphical representation of the cation ratio *CR* versus the condensation degree κ for the ternary compound classes *AE*–Si–N (blue) and *AE*–P–N (red), as well as for quaternary *AE*–(Si, P)–N (beige) as the region between both curves (*AE* = Ca, Sr, Ba). All literature known compounds, including the new compounds $Sr_2SiP_2N_6$ and $Sr_5Si_2P_6N_{16}$ are marked as symbols. For a full list refer to Table S2 (Supporting Information). The expanded view in the inset shows all compounds with $\kappa = 0.5$, differing in *CR*.

$$\kappa = \frac{N(NFC)}{N(LIG)} \tag{1}$$

$$CR = \frac{N(CC)}{N(NFC)} \tag{2}$$

where *N* is the count, *NFC* is the network-forming cation (Si, P), *LIG* is the ligand (N), and *CC* is the counter cation (Ca, Sr, Ba).

Mathematical transformations reveal the analytical relationship between the two parameters with respect to the oxidation states (*Ox*):

$$CR\ (\kappa) = -\frac{Ox(LIG)}{Ox(CC)} \cdot \frac{1}{\kappa} - \frac{Ox(NFC)}{Ox(CC)} \tag{3}$$

More details about the mathematical derivation can be found in the Supporting Information. While all ternary nitrides align with respective hyperbolic curves (blue and red), quaternary *AE*–(Si, P)–N can span the full region (beige) between both curves. For the latter, *Ox*(*NFC*) depends on the percentage composition of (Si, P) that is $CR(\kappa)$ can vary between the edge cases *Ox*(Si) = 4 and *Ox*(P) = 5. To date, this compositional space remains largely unexplored, with only one representative, namely $AESiP_3N_7$ (*AE* = Sr, Ba).[13] The challenging synthesis, either requiring NH_4F assisted high-pressure high-temperature conditions or molecular precursors, explains this uncharted territory. The crystallochemical similarities of Si^{4+} and P^{5+}, in terms of charge, ionic radius, and atomic scattering factor, complicate structure elucidation.[14,15] This is also the reason why Eisenburger et al. employed scanning transmission electron microscopy (STEM) to determine the partially ordered nature of their network. There are other related (Si, P)–N compounds, such as the disordered wurtzite type $SiPN_3$, or SiP_2N_4NH and $AESi_3P_4N_{10}(NH)_2$ (*AE* = Mg, Ca, Sr), where Si occupies octahedra and P tetrahedra.[16–18] However, there are no reports of ordered and disordered (Si, P)–N networks in which Si and P form an anionic, tetrahedral network. Consequently, we introduce $Sr_2SiP_2N_6$ as the first ordered and $Sr_5Si_2P_6N_{16}$ as the first disordered representatives of anionic (Si, P)–N networks in this study, respectively.

2. Results and Discussion

2.1. Synthesis

Both compounds $Sr_2SiP_2N_6$ and $Sr_5Si_2P_6N_{16}$ were prepared via the azide route at 3 GPa and 1400 °C in a multianvil press starting from $Sr(N_3)_2$, amorphous Si_3N_4, and α-P_3N_5. For luminescence experiments, we added 1–3 mol.% EuN with respect to Sr^{2+}. Due to their similar compositions, the products typically occur as microcrystalline powder mixtures, distinguishable by their crystal shape and luminescence (Figures S1 and S2, Supporting Information). The products, like many highly condensed nitrides ($\kappa \geq 0.5$), are stable toward moisture and air.

2.2. Structure Elucidation

The similarities between Si and P make the structure elucidation a multistep process when both occupy the same sites in the crystal. Therefore, it is difficult to determine the network based on single-crystal X-ray diffraction data alone. The same applies to O and N as ligands. Even though we did not include oxygen, potential contamination by diffusion in a multianvil press needs to be considered. We followed a four-step workflow: 1) Determination of a preliminary structure model from single-crystal X-ray data of the form $Sr_x(Si, P)_y(N, O)_z$. 2) Determination of the chemical composition by measuring EDX on flat single-crystal surfaces. 3) Determination of tetrahedral occupancies by STEM EDX. 4) Finalization of the structure model by implementing occupational results from steps (2) and (3).

$Sr_2SiP_2N_6$ crystallizes in the structure type of $K_2ZnSi_2O_6$ in the non-centrosymmetric space group $C222_1$ (no. 20) with $a = 6.0849(1)$, $b = 8.8203(2)$, $c = 10.2500(2)$ Å, and *Flack parameter* $x = -0.017(6)$.[19,20] Further crystallographic data are given in Tables S3–S5 (Supporting Information). We confirmed the absence of centrosymmetry by measuring the second harmonic generation (SHG) intensities on a powder sample with grain sizes below 30 µm. The value of 31(11) mV is comparable to that of quartz with 24(4) mV (< 5 µm). The preliminary empirical formula from single-crystal X-ray data was $Sr_2(Si, P)_3(N, O)_6$. Single-crystal EDX measurements, averaged over ten points, gave a composition of Sr 18(1), Si 11(1), P 18(1), N 51(1), and O 3(1) at%, corresponding to a refined empirical formula $Sr_2Si_{1+x}P_{2-x}N_{6-x}O_x$ ($x \approx 0.1$). Given the isoelectronic relationship between Si–O and P–N, we consider oxygen impurities to this extent to be entropy-driven and hardly avoidable in a multianvil press, justifying the idealized sum formula of $Sr_2SiP_2N_6$. The structure itself consists of a highly condensed network of Q^2 tetrahedra with condensation degree $\kappa = 0.5$ (**Figure 2**). *T2* tetrahedra (green) form single chains along [001], with all chains being cross-linked by *T*1 tetrahedra (yellow). The Sr^{2+} ions occupy a single crystallographic site with (6+3)-fold coordination through N^{3-} which can be described as a distorted tricapped trigonal prism (Johnson body 51) with a

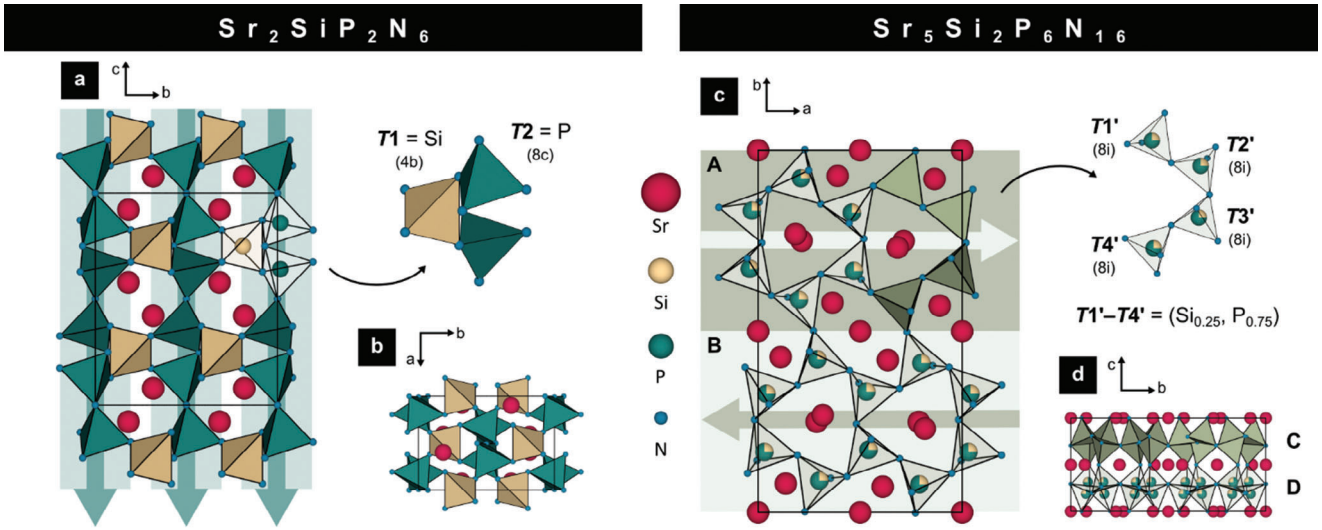

Figure 2. Crystal structure of $Sr_2SiP_2N_6$ in a) [100] and b) [001] showing an ordered tetrahedral network of P (*T*2, green) single chains which are cross-linked by Si (*T*1, yellow) tetrahedra. The crystal structure of $Sr_5Si_2P_6N_{16}$ in c) [001] shows alternating double-chains along [010] in ABAB sequence. The tetrahedra *T*1'–*T*4' are occupied by ($Si_{0.25}$, $P_{0.75}$) building a disordered network. In d) the ABAB layers are stacked along [001] in CDCD sequence with D being the inverse of C.

volume of $V = 42.4$ Å^3.[21] To determine the occupancy of *T*1 and *T*2 sites, we used scanning transmission electron microscopy on an atomic scale. In the first step, we oriented the crystal along a crystallographic axis in which we could study the tetrahedral Wyckoff positions separately, for $Sr_2SiP_2N_6$ this was the direction [100]. In the second step, we chose an area scan to measure a two-dimensional EDX map as highlighted in yellow in **Figure 3**. By integration over the EDX signal, we obtained a sinusoid where each maximum indicates the presence of the corresponding element at that position. For $Sr_2SiP_2N_6$, the signals of Si and P oscillate out of phase, which means that Si is only present when P is not and vice versa. It was possible to assign the tetrahedral positions $T1 = Si^{4+}$ and $T2 = P^{5+}$ and refine a final structure model, where $Sr_2SiP_2N_6$ comprises the first ordered (Si, P)–N network. We were able to corroborate the structure model by Raman spectroscopy, where the simulated spectrum shows very good

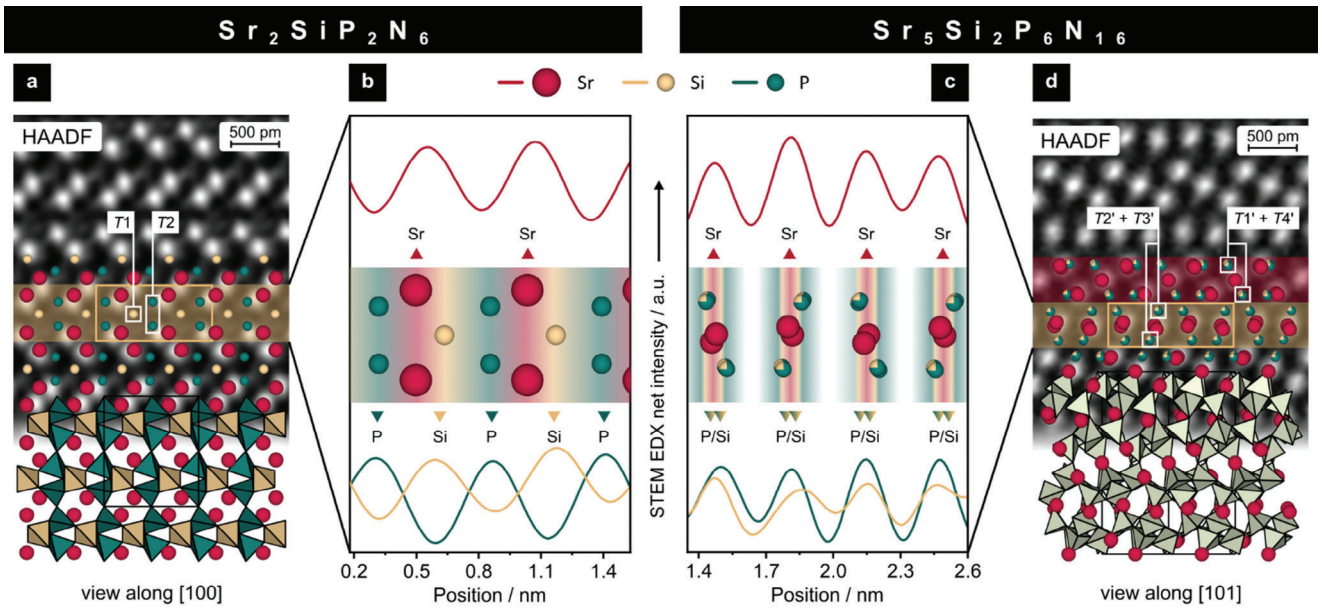

Figure 3. STEM high-angle annular dark-field (HAADF) images with structure overlay of a) $Sr_2SiP_2N_6$ and d) $Sr_5Si_2P_6N_{16}$. STEM EDX area scans are highlighted in yellow. For the area scan highlighted in red, please refer to Figure S3 (Supporting Information). The integrated EDX signals of the area scans show out of phase oscillation of the Si (yellow) and P (green) signals for b) $Sr_2SiP_2N_6$ and in-phase oscillation for c) $Sr_5Si_2P_6N_{16}$, indicating an ordered network for $Sr_2SiP_2N_6$ and ruling out an ordered network for $Sr_5Si_2P_6N_{16}$. The Sr (red) EDX signal serves as a position reference.

agreement with the experimental spectrum (Figure S8, Supporting Information).

For the second compound $Sr_5Si_2P_6N_{16}$, the same workflow was chosen. Single-crystal X-ray diffraction data yielded a preliminary formula $Sr_5(Si, P)_8(N, O)_{16}$ and, in combination with EDX measurements, an experimental sum formula of $Sr_5Si_{2+x}P_{6-x}N_{16-x}O_x$ with $x \approx 0.7$ (Sr 18(1), Si 10(1), P 19(1), N 48(1), and O 4(1) at%). It crystallizes in the centrosymmetric space group *Pbam* (no. 55) with lattice parameters $a = 9.9136(2)$, $b = 17.5676(3)$, and $c = 8.39680(10)$ Å.[20] Further crystallographic data are given in Tables S3, S6, and S7 (Supporting Information). In agreement with Liebau's classification of silicates, the fundamental building block of this network is best described as an unbranched double-chain along [100] comprising four distinct tetrahedral positions *T*1'–*T*4' (Figure 2).[22] These double chains alternate along [010] in A–B–A–B sequence. The layers repeat along [001] in C–D–C–D sequence, forming a complex three-dimensional network of Q^2 tetrahedra with condensation degree $\kappa = 0.5$, analogous to $Sr_2SiP_2N_6$. Unlike in $Sr_2SiP_2N_6$, the Sr^{2+} ions in $Sr_5Si_2P_6N_{16}$ occupy not one but six crystallographic sites, which differ considerably in terms of coordination and polyhedral volume ($CN = 6$–13, $V = 18.3$–68.5 Å^3). Coordination polyhedra were determined using the Charge Distribution method.[23] Tetrahedral occupancies were further investigated for this network using atomic resolution STEM EDX. In the case of $Sr_5Si_2P_6N_{16}$, the available viewing direction [101] did not match an ideal viewing direction, e.g., [001]. That means, we examined the tetrahedral sites in doublets of *T*1'+*T*4' and *T*2'+*T*3' rather than individually. This can be attributed to both the sample, e.g., preferred crystal orientations and textures, and constraints of the setup, e.g., limited rotational degrees of freedom. We measured two separate STEM EDX area scans for both doublets, highlighted in yellow (*T*2'+*T*3') and red (*T*1'+*T*4') in Figure 3. They show in-phase EDX signals for Si and P in both cases, suggesting that the (Si, P)–N network is not ordered. This becomes clear when we consider the Si:P ratio of 1:3 in $Sr_5Si_2P_6N_{16}$ and the four available tetrahedral sites. Only one doublet would show a Si signal regardless of the ordering variant. Only an undetected superstructure would show similar signals, for which there is no evidence on the precession images (Figure S9, Supporting Information). Nevertheless, the absence of order is not proof of disorder in a network. Eisenburger et al. recently reported a highly condensed (Si, P)–N network with partial order in $AESiP_3N_7$ (*AE* = Sr, Ba), where *T*1* is fully occupied by P and *T*2* by ($Si_{0.5}$, $P_{0.5}$).[13] Based on our STEM EDX data, it is not possible to distinguish the disordered from the partially ordered network since the EDX signal of Si and P can only be evaluated qualitatively.

2.3. Low-Cost Crystallographic Calculations

To determine the tetrahedral occupancies of $Sr_5Si_2P_6N_{16}$, we analyzed the ordered (A), partially ordered (B), and disordered (C) network variants (**Figure 4**) by low-cost crystallographic calculations. After refining each variant based on the single-crystal X-ray data, we calculated the Ewald site energies, charge distributions (CHARDI), bond valence sums (BVS), polyhedral volumes, and distances of all crystallographic (Si, P)–N sites.[24–30] Since there were insufficient reference data for mixed (Si, P)–N networks,

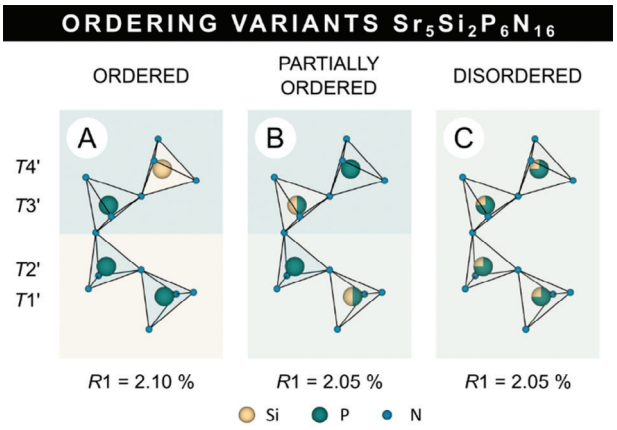

Figure 4. Ordering variants of $Sr_5Si_2P_6N_{16}$ with A) full ordering, B) partial ordering, and C) disordering of all tetrahedral sites *T*1'–*T*4'. The refinements yield very similar *R*1 values for all cases.

the idea was that we could calculate expected values from literature data of pure Si–N and P–N networks, proportional to their percentage composition. As an example, the volume of a ($Si_{0.25}$, $P_{0.75}$)–N_4 tetrahedron is calculated as:

$$\langle V \rangle \left((Si_{0.25}, P_{0.75}) - N_4 \right) = 0.25 \cdot \bar{V} \left(Si - N_4 \right) + 0.75 \cdot \bar{V} \left(P - N_4 \right) \quad (4)$$

where $\langle V \rangle$ is the expected volume and $\bar{V}$ is the average volume calculated from literature.

The expected values can be used to calculate the percentage deviation of the different ordering variants for each method. In this way, the variant with the lowest mean percentage deviation is the most probable. This approach is based on several assumptions: 1) All structure models used are of sufficiently good quality, since all methods depend strongly on interatomic distances. 2) All networks are predominantly ionic, justifying the use of point charge concepts such as Ewald summation and CHARDI. 3) Our (Si, P)–N networks can be described as a combination of Si–N and P–N networks and, therefore, allow for the definition of expected values. 4) The differences in charge, size, and atomic scattering factor of Si^{4+} and P^{5+} lead to significant structural changes observable by single-crystal X-ray diffraction.

Based on these assumptions, an appropriate group of literature compounds was selected. A full list is found in Table S1 (Supporting Information). The results of all methods and ordering variants of $Sr_5Si_2P_6N_{16}$ are shown in **Figure 5**. The disordered variant (C) showed the lowest mean deviation $\bar{D}$ of 1.0 %, followed by the partially ordered variant (B) with 3.3 % and the ordered variant (A) with 5.2 %. This is consistent with the results from STEM EDX, where (A) has already been excluded. The deviations from both (B) and (C) are within the range of literature compounds, but $\bar{D}$(B) more than triples compared to $\bar{D}$(C) despite comparatively small changes in the tetrahedral composition. Furthermore, not only does the mean deviation increase from (C) to (B), but all individual methods show the same trend. Although partial ordering was observed in $AESiP_3N_7$ (*AE* = Sr, Ba), most compounds exhibit either ordered or disordered networks,

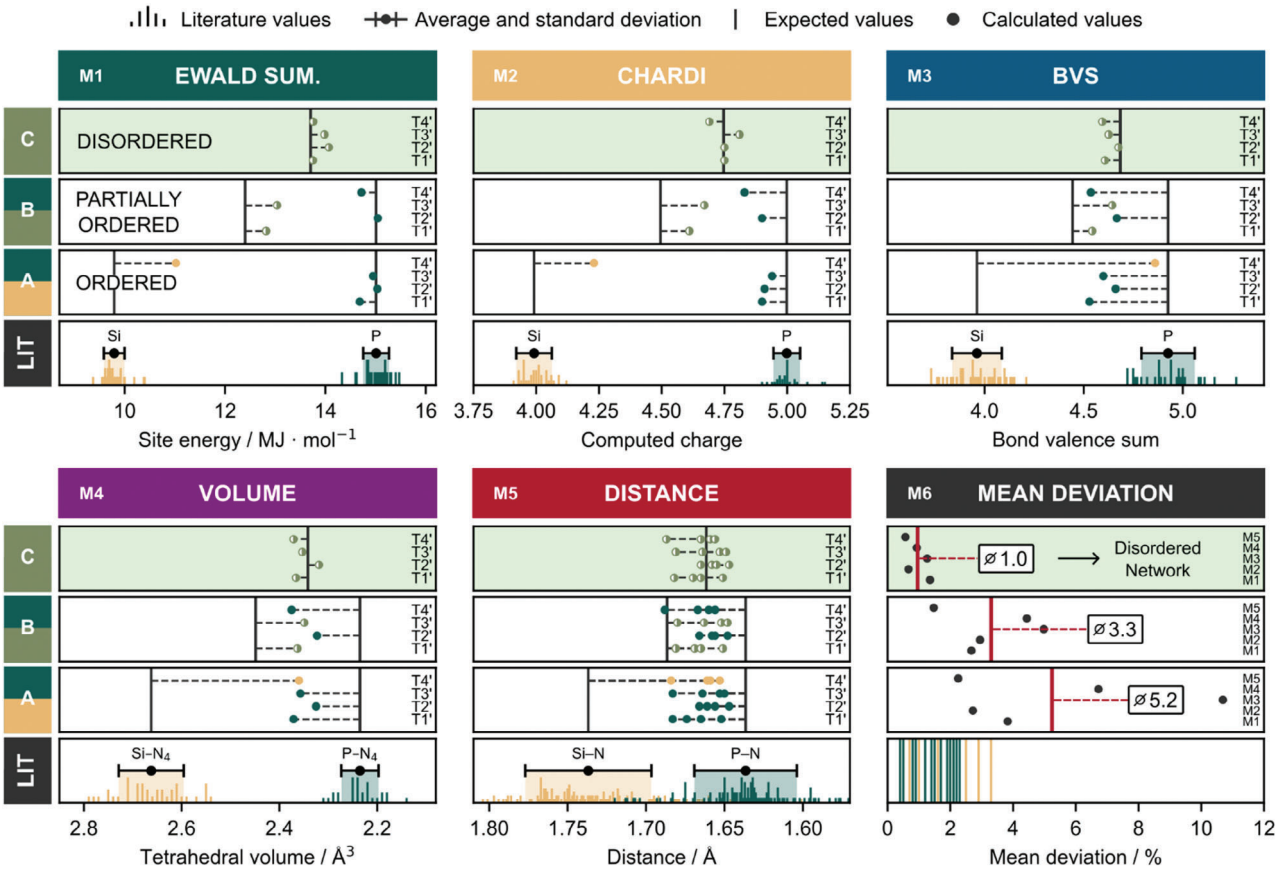

Figure 5. Comparison of all ordering variants A)–C) of $Sr_5Si_2P_6N_{16}$ by low-cost crystallographic calculations that is Ewald site energies, CHARDI, BVS, tetrahedral volumes, and distances. For each method, we considered the occupation of all tetrahedral positions *T*1'–*T*4' separately, with Si (yellow), P (green), and mixed (Si, P) (olive green). The ordering variant with the lowest mean percentage deviation from the expected values that were calculated from literature (LIT) gives the most probable solution. LIT values are given in relative frequency.

supporting the need to consider partial ordering without overestimating its probability. Based on our data, we claim, that $Sr_5Si_2P_6N_{16}$ is the first anionic, disordered (Si, P)–N network. For completeness, we also analyzed plausible ordering variants of the other compound $Sr_2SiP_2N_6$ by crystallographic calculations. Here, the ordered variant showed the smallest mean deviation of 1.1 %, while the partially ordered variant ($\overline{D}$ = 8.5 %) and disordered variant ($\tilde{D}$ = 5.5 %) were considerably less congruent (Figures S10 and S11, Supporting Information). This is in line with our STEM EDX experiment that has already confirmed the ordered nature of the (Si, P)–N network in $Sr_2SiP_2N_6$.

2.4. Luminescence

After doping with Eu^{2+}, $Sr_2SiP_2N_6$:Eu^{2+} and $Sr_5Si_2P_6N_{16}$:Eu^{2+}, show cyan and orange luminescence upon irradiation with ultraviolet light, respectively. We measured the photoluminescence (PL) and photoluminescence excitation spectra (PLE, **Figure 6**a) on individual particles (**Figure 7**). $Sr_2SiP_2N_6$:Eu^{2+} emits in the cyan region with a maximum at 506 nm (*M*1) and a full width at half maximum *fwhm* = 60 nm/2311 cm^{-1}. The narrow emission is consistent with only one Sr site available for doping by Eu^{2+}. In contrast, we observe a broad emission in the PL spectrum of $Sr_5Si_2P_6N_{16}$:Eu^{2+} starting at ≈500 nm and extending over the entire spectral range with three maxima at 534 (*M*2), 662 (*M*3, *fwhm* = 110 nm/2501 cm^{-1}), and 745 nm (*M*4). This indicates multiple distinct activator environments and is consistent with the six chemically different Sr sites in $Sr_5Si_2P_6N_{16}$:Eu^{2+}. In principle, all sites are suitable for Eu^{2+}-doping with respect to their volume *V* = 18.3–68.5 $Å^3$.[4,31] Reliable assignment of Sr sites to emission bands is possible only with theoretical calculations of the crystal fields and excited states of Eu^{2+} ($4f^6 5d^1$).[32] Nevertheless, a comparison of the Sr sites in terms of their weighted mean Sr–N distances (*WMD*(Sr–N)), effective coordination numbers (*ECoN*), and site symmetries can contribute to a better understanding of such a spectrum.[23,26] We expect that the smaller *WMD*(Sr–N) or the higher *ECoN*, the larger the Stokes shift, which is due to the stronger splitting of the ligand field. In contrast, the higher the site symmetry, the smaller the Stokes shift, because higher symmetry means fewer degrees of freedom for structural relaxation. With this in mind, we divided Sr1'–Sr6' into four groups to assign them to maxima *M*2–*M*4: 1) Sr6' does not contribute to any of the visible maxima. We argue that due to the largest weighted mean distance *WMD*(Sr6'–N) = 2.89 Å and *ECoN* = 9.64 its emission should be expected in the blue region.

Therefore, its absence can be explained by the chosen excitation wavelength (λ_{exc} = 460 nm), which is too large. 2) Sr2'

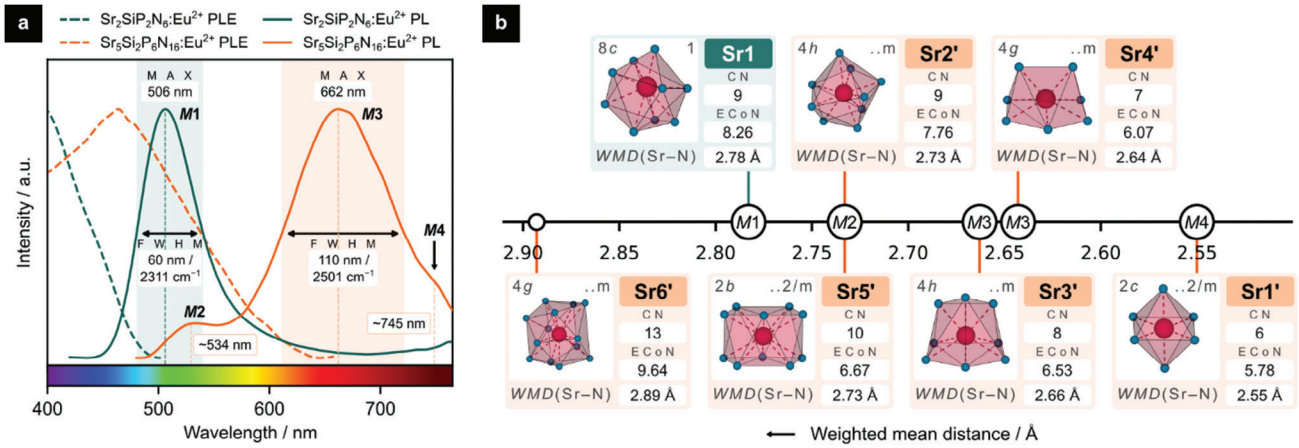

Figure 6. a) Photoluminescence excitation (PLE, dashed) and photoluminescence (PL, solid) spectra of $Sr_2SiP_2N_6:Eu^{2+}$ (green) and $Sr_5Si_2P_6N_{16}:Eu^{2+}$ (orange). $Sr_2SiP_2N_6:Eu^{2+}$ shows an emission maximum (*M*1) at 506 nm. $Sr_5Si_2P_6N_{16}:Eu^{2+}$ has three emission bands at 534 (*M*2), 662 (*M*3), and 745 nm (*M*4). We smoothed the data with a Gaussian filter ($\sigma = 2$). Unfiltered spectra are provided in Figure S12 (Supporting Information). b) Comparison of the coordination environment of possible activator sites with respect to their weighted mean Sr–N distances (*WMD*).

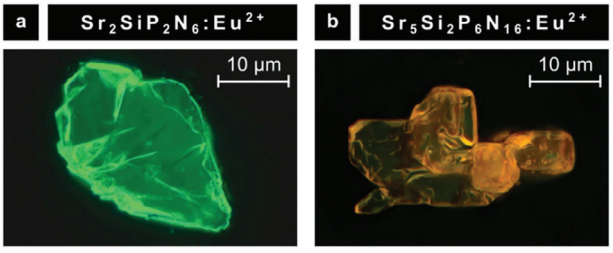

Figure 7. Luminescence micrographs of individual particles of a) $Sr_2SiP_2N_6:Eu^{2+}$ and b) $Sr_5Si_2P_6N_{16}:Eu^{2+}$, excited at 395 nm.

and Sr5' were assigned to maximum *M*2 because they have significantly larger environments (*WMD*(Sr2'–N) = *WMD*(Sr5'–N) = 2.73 Å, *ECoN*(Sr2') = 7.76, *ECoN*(Sr5') = 6.67) than Sr3' and Sr4' (*WMD*(Sr3'–N) = 2.66, *WMD*(Sr4'–N) = 2.64 Å, *ECoN*(Sr3') = 6.53, *ECoN*(Sr4') = 6.07). We expect additional splitting of *M*2 despite the identical weighted mean distances since Sr5' has a lower effective coordination number and higher symmetry than Sr2', two factors that will reduce the Stokes shift. However, due to the low intensity of *M*2, which we attribute to reabsorption effects and poor excitation at 460 nm, no further conclusions were drawn from the spectrum. 3) The gradual slope of *M*3 suggests a superposition of several similar emission maxima. This fits well with Sr3' and Sr4' which have similar *WMD* and *ECoN* values (*WMD*(Sr3'–N) = 2.66, *WMD*(Sr4'–N) = 2.64 Å, *ECoN*(Sr3') = 6.53, *ECoN*(Sr4') = 6.07) as well as the same site symmetry. 4) Sr1' has the smallest coordination environment with *WMD*(Sr1'–N) = 2.55 and *ECoN* = 5.78, significantly smaller than those of Sr3' and Sr4'. Despite the higher site symmetry of 2/*m*, we expect for Sr1' the strongest Stokes shift that yields *M*4.

3. Conclusion

We successfully synthesized two novel strontium nitridosilicate phosphates, namely $Sr_2SiP_2N_6$ and $Sr_5Si_2P_6N_{16}$, via the azide route at 3 GPa and 1400 °C in a multianvil press. Using a four-step workflow adapted to mixed tetrahedral networks, we identified the structure of $Sr_2SiP_2N_6$, which reveals an unprecedented ordered (Si, P)–N network. The second compound, $Sr_5Si_2P_6N_{16}$, presented more challenges. Combining STEM EDX data with low-cost crystallographic calculations provided evidence for a disordered (Si, P)–N network, which is the first of its kind to be reported. We introduced the dopant Eu^{2+} into both compounds to investigate their luminescence properties. $Sr_2SiP_2N_6:Eu^{2+}$ shows a narrow emission in the cyan region at 506 nm (*fwhm* = 60 nm/2311 cm^{-1}), consistent with the structure having only one Sr site available for Eu^{2+} doping. $Sr_5Si_2P_6N_{16}:Eu^{2+}$ shows a broad emission with three maxima at 534, 662, and 745 nm, where we suggested an assignment of Sr sites to the emission bands. In summary, our research represents a significant advance in the understanding of mixed (Si, P)–N networks, as we have been able to demonstrate their variability in two examples. Despite the same condensation degree and very similar stoichiometries, both compounds exhibit fundamentally different structures and luminescence properties, ranging from cyan to orange. Future investigations should further explore the compositional space of mixed networks with similar network-forming cations, e.g., (Si, P), (Al, Si), or (Mg, Si), especially with respect to their luminescence properties.

Supporting Information

Supporting Information is available from the Wiley Online Library or from the author.

Acknowledgements

The authors gratefully thank Christian Minke (Department of Chemistry, LMU Munich) for the EDX measurements and SEM images. Massimo Nespolo (CRM, Université de Lorraine) and Corrado Cuocci (Institute of Crystallography, CNR) deserve thanks for their support with the CHARDI-2015 and EXPO2014 programs. M.D. also thanks the Bundesministerium für Bildung und Forschung (BMBF) for financial support.

Open access funding enabled and organized by Projekt DEAL.

Conflict of Interest

The authors declare no conflict of interest.

Data Availability Statement

The data that support the findings of this study are available in the supplementary material of this article.

Keywords

luminescence, mixed networks, nitrides, nitridosilicate phosphates, STEM EDX

Received: October 23, 2023
Published online:

[1] S. Li, R.-J. Xie, T. Takeda, N. Hirosaki, *ECS J. Solid State Sci. Technol.* **2017**, *7*, R3064.
[2] R.-J. Xie, N. Hirosaki, *Sci. Technol. Adv. Mater.* **2007**, *8*, 588.
[3] R.-J. Xie, N. Hirosaki, H.-L. Li, Y. Q. Li, M. Mitomo, *J. Electrochem. Soc.* **2007**, *154*, J314.
[4] K. Uheda, N. Hirosaki, Y. Yamamoto, A. Naito, T. Nakajima, H. Yamamoto, *Electrochem. Solid-State Lett.* **2006**, *9*, H22.
[5] P. Pust, V. Weiler, C. Hecht, A. Tücks, A. S. Wochnik, A.-K. Henß, D. Wiechert, C. Scheu, P. J. Schmidt, W. Schnick, *Nat. Mater.* **2014**, *13*, 891.
[6] G. J. Hoerder, M. Seibald, D. Baumann, T. Schröder, S. Peschke, P. C. Schmid, T. Tyborski, P. Pust, I. Stoll, M. Bergler, C. Patzig, S. Reißaus, M. Krause, L. Berthold, T. Höche, D. Johrendt, H. Huppertz, *Nat. Commun.* **2019**, *10*, 1824.
[7] P. Pust, S. Pagano, W. Schnick, *Eur. J. Inorg. Chem.* **2013**, *7*, 1157.
[8] P. Wagatha, V. Weiler, P. J. Schmidt, W. Schnick, *Chem. Mater.* **2018**, *30*, 1755.
[9] P. Pust, A. S. Wochnik, E. Baumann, P. J. Schmidt, D. Wiechert, C. Scheu, W. Schnick, *Chem. Mater.* **2014**, *26*, 3544.
[10] Q. Wu, Y. Li, C. Wang, J. Luo, *J. Lumin.* **2018**, *201*, 485.
[11] S. Schmiechen, H. Schneider, P. Wagatha, C. Hecht, P. J. Schmidt, W. Schnick, *Chem. Mater.* **2014**, *26*, 2712.
[12] R. M. Pritzl, N. Prinz, P. Strobel, P. J. Schmidt, D. Johrendt, W. Schnick, *Chem. - Eur. J.* **2023**, *29*, e202301218.
[13] L. Eisenburger, O. Oeckler, W. Schnick, *Chem. - Eur. J.* **2021**, *27*, 4461.
[14] R. D. Shannon, *Acta Crystallogr., Sect. A: Found. Crystallogr.* **1976**, *32*, 751.
[15] P. J. Brown, A. G. Fox, E. N. Maslen, M. A. O'Keefe, B. T. M. Willis, in *International Tables for Crystallography Volume C: Mathematical, Physical and Chemical Tables* (Ed: E. Prince), Springer, Netherlands, Dordrecht **2004**, p. 554.
[16] H. P. Baldus, W. Schnick, J. Luecke, U. Wannagat, G. Bogedain, *Chem. Mater* **1993**, *5*, 845.
[17] S. Vogel, A. T. Buda, W. Schnick, *Angew. Chem., Int. Ed.* **2019**, *58*, 3398.
[18] L. Eisenburger, P. Strobel, P. J. Schmidt, T. Bräuniger, J. Wright, E. L. Bright, C. Giacobbe, O. Oeckler, W. Schnick, *Angew. Chem., Int. Ed.* **2022**, *61*, e202114902.
[19] A. R. Hogrefe, M. Czank, *Acta Crystallogr.* **1995**, *51*, 1728.
[20] Deposition Numbers 2301100 and 2301110 contain the supplementary crystallographic data for this paper. These data are provided free of charge by the joint Cambridge Crystallographic Data Centre and Fachinformationszentrum Karlsruhe Access Structures service.
[21] N. W. Johnson, *Can. J. Math.* **1966**, *18*, 169.
[22] F. Liebau, *Z. Phys. Chem.* **1956**, *206O*, 73.
[23] R. Hoppe, *Z. Kristallogr. - Cryst. Mater.* **1979**, *150*, 23.
[24] A. Y. Toukmaji, J. A. Board, *Comput. Phys. Commun.* **1996**, *95*, 73.
[25] M. Nespolo, *Acta Crystallogr* **2016**, *72*, 51.
[26] M. Nespolo, B. Guillot, *J. Appl. Crystallogr.* **2016**, *49*, 317.
[27] A. Altomare, C. Cuocci, C. Giacovazzo, A. Moliterni, R. Rizzi, N. Corriero, A. Falcicchio, *J. Appl. Crystallogr.* **2013**, *46*, 1231.
[28] K. Momma, F. Izumi, *J. Appl. Crystallogr.* **2011**, *44*, 1272.
[29] L. Link, R. Niewa, *J. Appl. Crystallogr.* **2023**, *56*, 1855.
[30] S. P. Ong, W. D. Richards, A. Jain, G. Hautier, M. Kocher, S. Cholia, D. Gunter, V. L. Chevrier, K. A. Persson, G. Ceder, *Comput. Mater. Sci.* **2013**, *68*, 314.
[31] G. Anoop, D. W. Lee, D. W. Suh, S. L. Wu, K. M. Ok, J. S. Yoo, *J. Mater. Chem. C* **2013**, *1*, 4705.
[32] R. Shafei, D. Maganas, P. J. Strobel, P. J. Schmidt, W. Schnick, F. Neese, *J. Am. Chem. Soc.* **2022**, *144*, 8038.
[33] A. Stock, H. Grüneberg, *Ber. Dtsch. Chem. Ges.* **1907**, *40*, 2573.
[34] R. Suhrmann, K. Clusius, *Z. Anorg. Allg. Chem.* **1926**, *152*, 52.
[35] D. Walker, M. A. Carpenter, C. M. Hitch, *Am. Mineral.* **1990**, *75*, 1020.
[36] D. C. Rubie, *Phase Transitions* **1999**, *68*, 431.
[37] H. Huppertz, *Z. Kristallogr. - Cryst. Mater.* **2004**, *219*, 330.
[38] E.-M. Bertschler, R. Niklaus, W. Schnick, *Chem. - Eur. J.* **2017**, *23*, 9592.
[39] M. Mallmann, S. Wendl, P. Strobel, P. J. Schmidt, W. Schnick, *Chem. - Eur. J.* **2020**, *26*, 6257.
[40] A. Marchuk, L. Neudert, O. Oeckler, W. Schnick, *Eur. J. Inorg. Chem.* **2014**, *21*, 3427.
[41] Bruker-AXS, APEX3, Version 2016.5-0, Karlsruhe, Germany, **2016**.
[42] SAINT, *Data Integration Software*, SAINT, Madison, WI **1997**.
[43] Bruker-AXS, *XPREP Reciprocal Space Exploration, Version 6.*, Vol. *12*, Bruker-AXS, Karlsruhe, Germany **2001**.
[44] G. M. Sheldrick, *SHELXS-97 Program of the Solution of Crystal Structure*, University of Göttingen, Göttingen **1997**.
[45] G. M. Sheldrick, *Acta Crystallogr C Struct Chem* **2015**, *71*, 3.
[46] L. J. Farrugia, *J. Appl. Crystallogr.* **2012**, *45*, 849.
[47] Gatan Inc., *DigitalMicrograph, Version 3.6.5*, Gatan Inc., Pleasanton, CA **1999**.
[48] J. L. Lábár, *Ultramicroscopy* **2005**, *103*, 237.
[49] Stadelmann, *jEMS Software Package, Version 3.60907U2011*, Stadelmann, Saas-Fee, Switzerland **2011**.
[50] Thermo Fisher Scientific, *Velox*, Thermo Fisher Scientific, Waltham, MA **2021**.
[51] T. Schlieper, W. Milius, W. Schnick, *Z. Anorg. Allg. Chem.* **1995**, *621*, 1380.
[52] F. Karau, W. Schnick, *Z. Anorg. Allg. Chem.* **2006**, *632*, 231.
[53] F. W. Karau, W. Schnick, *J. Solid State Chem.* **2005**, *178*, 135.
[54] H. Huppertz, W. Schnick, *Chem. - Eur. J.* **1997**, *3*, 249.
[55] S. Vogel, M. Bykov, E. Bykova, S. Wendl, S. D. Kloß, A. Pakhomova, N. Dubrovinskaia, L. Dubrovinsky, W. Schnick, *Angew. Chem., Int. Ed.* **2020**, *59*, 2730.
[56] P. Eckerlin, *Z. Anorg. Allg. Chem.* **1967**, *353*, 225.
[57] S. Wendl, S. Mardazad, P. Strobel, P. J. Schmidt, W. Schnick, *Angew. Chem., Int. Ed.* **2020**, *132*, 18397.
[58] S. R. Römer, C. Braun, O. Oeckler, P. J. Schmidt, P. Kroll, W. Schnick, *Chem. - Eur. J.* **2008**, *14*, 7892.
[59] M. Zeuner, S. Pagano, S. Hug, P. Pust, S. Schmiechen, C. Scheu, W. Schnick, *Eur. J. Inorg. Chem.* **2010**, *2010*, 4945.
[60] F. J. Pucher, A. Marchuk, P. J. Schmidt, D. Wiechert, W. Schnick, *Chem. - Eur. J.* **2015**, *21*, 6443.
[61] S. D. Kloß, N. Weidmann, R. Niklaus, W. Schnick, *Inorg. Chem.* **2016**, *55*, 9400.
[62] K. Landskron, W. Schnick, *J. Solid State Chem.* **2001**, *156*, 390.
[63] P. Strobel, V. Weiler, P. J. Schmidt, W. Schnick, *Chem. - Eur. J.* **2018**, *24*, 7243.
[64] H. Jacobs, R. Nymwegen, *Z. Anorg. Allg. Chem.* **1997**, *623*, 429.

[65] S. Lupart, M. Zeuner, S. Pagano, W. Schnick, *Eur. J. Inorg. Chem.* **2010**, *2010*, 2636.
[66] S. D. Kloß, W. Schnick, *Angew. Chem., Int. Ed.* **2015**, *54*, 11250.
[67] M. Mallmann, C. Maak, R. Niklaus, W. Schnick, *Chem. - Eur. J.* **2018**, *24*, 13963.
[68] R. J. Bruls, H. T. Hintzen, R. Metselaar, C.-K. Loong, *J. Phys. Chem. Solids* **2000**, *61*, 1285.
[69] K. Landskron, S. Schmid, W. Schnick, *Z. Anorg. Allg. Chem.* **2001**, *627*, 2469.
[70] H. Jacobs, H. Mengis, *Eur. J. Solid State Inorg. Chem.* **1993**, *30*, 45.
[71] S. Wendl, W. Schnick, *Chem. - Eur. J.* **2018**, *24*, 15889.
[72] G. Pilet, H. A. Höppe, W. Schnick, S. Esmaeilzadeh, *Solid State Sci.* **2005**, *7*, 391.
[73] N. E. Brese, M. O'keeffe, *Acta Crystallogr* **1991**, *47*, 192.
[74] S. K. Kurtz, T. T. Perry, *J. Appl. Phys.* **1968**, *39*, 3798.
[75] L. Bayarjargal, C.-J. Fruhner, N. Schrodt, B. Winkler, *Phys. Earth Planet. Inter.* **2018**, *281*, 31.
[76] P. Hohenberg, W. Kohn, *Phys. Rev. B* **1964**, *136*, B864.
[77] S. J. Clark, M. D. Segall, C. J. Pickard, P. J. Hasnip, M. I. J. Probert, K. Refson, M. C. Payne, *Z. Kristallogr. - Cryst. Mater.* **2005**, *220*, 567.
[78] J. P. Perdew, K. Burke, M. Ernzerhof, *Phys. Rev. Lett.* **1996**, *77*, 3865.
[79] K. Lejaeghere, G. Bihlmayer, T. Björkman, P. Blaha, S. Blügel, V. Blum, D. Caliste, I. E. Castelli, S. J. Clark, A. Dal Corso, S. De Gironcoli, T. Deutsch, J. K. Dewhurst, I. Di Marco, C. Draxl, M. Dułak, O. Eriksson, J. A. Flores-Livas, K. F. Garrity, L. Genovese, P. Giannozzi, M. Giantomassi, S. Goedecker, X. Gonze, O. Grånäs, E. K. U. Gross, A. Gulans, F. Gygi, D. R. Hamann, P. J. Hasnip, et al., *Science* **2016**, *351*, 6280.
[80] H. J. Monkhorst, J. D. Pack, *Phys. Rev. B* **1976**, *13*, 5188.
[81] S. Grimme, J. Antony, S. Ehrlich, H. Krieg, *J. Chem. Phys.* **2010**, *132*, 154104.
[82] K. Refson, P. R. Tulip, S. J. Clark, *Phys. Rev. B* **2006**, *73*, 155114.
[83] K. Miwa, *Phys. Rev. B* **2011**, *84*, 094304.
[84] H. Yamane, H. Morito, *Inorg. Chem.* **2013**, *52*, 5559.
[85] F. Ottinger, R. Nesper, *Z. Anorg. Allg. Chem.* **2005**, *631*, 1597.
[86] H. Yamane, F. J. Disalvo, *J. Alloys Compd.* **1996**, *240*, 33.
[87] Z. A. Gál, P. M. Mallinson, H. J. Orchard, S. J. Clarke, *Inorg. Chem.* **2004**, *43*, 3998.
[88] S. Wendl, L. Eisenburger, P. Strobel, D. Günther, J. P. Wright, P. J. Schmidt, O. Oeckler, W. Schnick, *Chem. - Eur. J.* **2020**, *26*, 7292.